JOURNAL OF PROPULSION AND POWER
Vol. 24, No. 2, March–April 2008

Time-Resolved Measurements of Impulse Generation in Pulsed Laser-Ablative Propulsion

Kohei Anju* and Keisuke Sawada†
Tohoku University, Sendai 980-8579, Japan
Akihiro Sasoh‡ and Koichi Mori§
Nagoya University, Nagaya 464-8603, Japan
and
Eugene Zaretsky¶
Ben-Gurion University of the Negev, 84105 Beer-Sheva, Israel

DOI: 10.2514/1.32017

Impulse generation mechanisms in pulsed laser ablation were experimentally studied using the velocity interferometer system for any reflector and framing Schlieren visualization. The impulse was estimated from the rear surface velocity at the center of the laser irradiated spot. The fluence was from 13 to 24 $\mathrm{J/cm^2}$. In most cases, the propulsive force generated even after the primary laser power peak significantly contributed to the total impulse. With the combination of transversely excited atmospheric CO_2 laser and aluminum target, only air breakdown was induced on the target surface without ablation and the impulse level was low. With decreasing ambient pressure P_0, the impulse also decreased, and eventually vanished. With the combination of Nd:YAG laser and aluminum target, the ablation jet contributed to impulse generation and the impulse did not vanish even at vanishing P_0. When a transversely excited atmospheric CO_2 laser pulse was directed onto the polyacetal target, the impulse increased by a factor of 10 in comparison with the aluminum target, yielding a momentum coupling coefficient exceeding 400 $\mu\mathrm{N \cdot s/J}$. When P_0 was at atmospheric pressure, the laser plasma shielded the target surface against the proceeding laser power transmission and the impulse saturated at a lower value than at $P_0 = 10^{-2}$ Pa.

Nomenclature

a_s	=	bulk sound speed in target, m/s
C_m	=	momentum coupling coefficient, Eq. (4), N · s/J
d	=	laser spot diameter, m
E	=	laser energy, J
I	=	laser intensity, $\mathrm{W/m^2}$
I_m	=	impulse area density, Eq. (2), Pa · s
$\bar{I}_m$	=	impulse area density, time averaged in τ_R, Eq. (2a), Pa · s
P_0	=	ambient pressure, Pa
t	=	time, s
u	=	velocity of target rear surface, m/s
δ	=	thickness of target, m
λ	=	wavelength of laser beam for ablation, m
ρ	=	density of target material, $\mathrm{kg/m^3}$
τ_{1D}	=	period defined by Eq. (3), s
τ_{FWHM}	=	full width at half-maximum of laser power peak, s
τ_R	=	reverberation period, s
τ_V	=	time resolution of velocity interferometer system for any reflector, s
ϕ	=	fluence, $\mathrm{J/m^2}$

Presented as Paper 4389 at the 38th AIAA Plasmadynamics and Lasers Conference, Miami, FL, 25–28 June 2007; received 7 May 2007; revision received 31 July 2007; accepted for publication 27 August 2007.

*Graduate student, Department of Aerospace Engineering, 6-6-2 Aramaki-Aza-Aoba; currently Micro Device Department-2, SONY Corporation, 1-7-1 Konan Minato-ku, Tokyo 108-0075, Japan.

†Professor, Department of Aerospace Engineering, 6-6-2 Aramaki-Aza-Aoba. Associate Fellow AIAA.

‡Professor, Department of Aerospace Engineering, Furo-cho, Chikusaku. Associate Fellow AIAA.

§Assistant Professor, Department of Aerospace Engineering, Furo-cho, Chikusaku. Member AIAA.

¶Professor, Department of Mechanical Engineering, Post Office Box 653.

I. Introduction

LASER propulsion [1] is a useful method for remotely generating a propulsion impulse to an object. When using laser ablation of solids, that is, in "ablative laser propulsion" [2], an impulse can be generated even in space [3–7]. Laser ablation can enhance a laser-induced impulse in the atmosphere because the ablation plume can contribute to increasing the effective working mass [8–11]. The ratio of the impulse to the laser energy is termed the "momentum coupling coefficient" C_m and is an important quantity in evaluating propulsion performance. Usually, in ablative laser propulsion, a maximum C_m is obtained when the peak laser intensity ranges from 10^7–10^9 $\mathrm{W/cm^2}$ [5,12,13]. This range is a couple of orders in magnitude lower than that found in other applications. Experiments in laser-induced shock compression [14–16] or flyer acceleration [17] are usually conducted in the laser intensity range greater than 10^{13} $\mathrm{W/cm^2}$. Underwater laser peening is most effective in the intensity range of 10^9 to 2×10^{10} $\mathrm{W/cm^2}$. In this range, laser-ablative pressure on metal targets has been measured [18–20] using the velocity interferometer system for any reflector (VISAR) [21]. Remo [22], using the VISAR, measured the particle velocity of metal or stony meteorite samples, which were sandwiched by windows, when being irradiated by a 1054 nm laser pulse of a peak intensity of about 10^9 $\mathrm{W/cm^2}$. However, in the lower intensity range for laser propulsion, VISAR data have not been widely reported in past work.

In space, a laser beam interacts with the target and the resulting ablation plume. The interaction involves complicated physical processes: electrical breakdown, phase change, ionization, laser power absorption, plume jet dynamics, heat conduction, radiative heat transfer, etc. In the presence of ambient air, the complexity becomes even greater because the air itself can absorb the laser energy, and shock and expansion waves are generated, inducing complicated flow dynamics. As a result, the impulse characteristics also become complicated. Pakhomov et al. [23] investigated the

effect of ambient air pressure on a laser-ablative impulse to an aluminum target by a transversely excited atmospheric (TEA) CO_2 laser pulse. The impulse was an increasing function of ambient pressure. Watanabe et al. [13], through their free-flight experiments, obtained complicated impulse performance data for polyacetal (POM) subjected to a TEA CO_2 laser pulse. In particular, when the fluence was about 20 J/cm^2, the impulse was larger at low ambient pressures than at the atmospheric pressure.

In most past studies, the laser propulsion impulse was commonly measured using a ballistic pendulum [24–27]. However, using this method, only a time-integrated value of propulsive force, that is an impulse, could be obtained. McMordie and Roberts [28] used a quartz gauge to measure pressure histories on an aluminum target irradiated with a TEA CO_2 laser pulse. Dufresne et al. [29] and Sterling et al. [30] used a carbon piezoresistive gauge and a piezoelectric force sensor, respectively, for the same purpose. However, the spatiotemporal resolutions of both of these measurements were modest. To better understand the impulse generation mechanics and associated physics, measurement with a high time resolution is necessary. This study is directed toward a better understanding of the impulse generation mechanisms in laser-ablative propulsion through time-resolved impulse measurement and flow visualization.

II. Apparatus and Methods

Figure 1 shows the schematic of the experimental setup. The material to be laser pulsed was made either of aluminum or polyacetal (POM), see Table 1. A square target 100 mm on a side was cleaned with ethanol, and introduced into the vacuum chamber (inner diameter 0.7 m, length 2.0 m). The vacuum chamber pressure P_0 was set from 10^{-2} to 10^5 Pa. The chamber was evacuated using a turbomolecular pump, which was in turn backed by a rotary pump. The target was sandwiched by an aluminum holder at its upper and lower sides. For visualization, the left and right sides were left free. A laser pulse was directed onto the front surface (upper surface in Fig. 1) of the target. The specifications of the pulse lasers are given in Table 2.

The rear surface of the target was irradiated with the probe beam from the VISAR, a continuous-wave $NdYVO_4$ laser light with wavelength 532 nm, power 200 mW, and spot diameter 0.2 mm. The reflected diffused light was collected by the VISAR. The rear surface of the POM target was coated with a sputter-deposited, 5-μm-thick aluminum layer to enhance reflectivity. The aluminum layer also blocked the VISAR optics from radiation emission from the laser plasma. Unless otherwise stated, the rear surface was free.

The ablation plume, and associated waves and flows were recorded with a framing Schileren system using a high-speed camera (ultra 8, DRS Hadland, Ltd.). The camera could capture eight 12-bit, 520×520 pixel, digital images with an image intensifier of 10^3 gain. The framing rate and exposure time, indicated in each figure, were controlled by the camera itself with the time resolution of 10 ns. As the light source, a flash lamp (effective duration 300 μs) was used. Near the focus, before imaging onto the camera, a circular iris was placed to act as a knife edge. The gray scale of the image qualitatively corresponds to the fluid density gradient along the radial direction measured from the image center. It should be noted that in some images, radiation emission from the laser plasma is superimposed.

The optical arrangement in the VISAR is shown in Fig. 2 [31]. When the rear surface of the target has a velocity u, the reflected light from the surface undergoes a Doppler shift. This Doppler-shifted light beam was introduced to the VISAR. In the VISAR, the reflected beam was split mainly into two beams. After traveling over different optical distances, the two beams merged and interfered, generating a beat signal. The optical delay was generated with a 580-mm-long water path. The fringe constant, which was obtained by taking into account the dispersion of refraction number in the water [32], was 99.8 m/s/fringe. The phase of the beat was obtained from the Lissajous figure, generated by the signals of the photomultiplier units PMU-A and PMU-B, each of which was normalized to that of PMU-C. The response and rise times of the photomultiplier units were 20 ns and 2 ns, respectively. The overall time resolution of the measurement τ_V was about 4 ns.

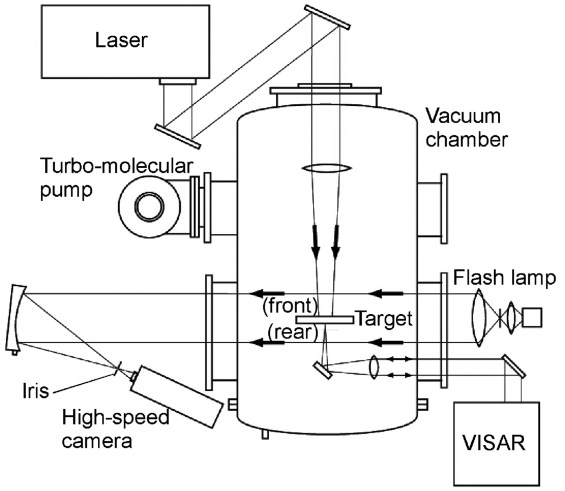

Fig. 1 Experimental setup.

Once the target experiences an impulse, longitudinal waves reverberate across the target layer. These reverberations are superimposed on the velocity history. The period of reverberation τ_R is given by

$$\tau_R = \frac{2\delta}{a_S} \tag{1}$$

where a_S denotes the bulk sound speed of the target. In the case of the aluminum target, $\tau_R \cong \tau_V$, see Table 1, the measured velocity approximately equals the velocity of the center of mass in the laser spot. Usually, in laser propulsion, an "impulse" is defined as the time-integration of a force, which in turn is obtained by spatially integrating a pressure over the laser irradiated spot area. In this paper, an "impulse area density I_m" is defined as the time-integration of a pressure, but is not spatially integrated. I_m is obtained by

$$I_m(t) = \rho_0 \delta u(t) \tag{2}$$

For the POM target, however, $\tau_R \gg \tau_V$; the reverberation signal is significantly superimposed on the signal of the center of mass velocity. In this case, an averaged impulse area density over a reverberation period $\bar{I}_m$ is calculated by averaging a temporal value, such that

$$\bar{I}_m\left(t + \frac{\tau_R}{2}\right) = \frac{\rho\delta}{\tau_R}\int_t^{t+\tau_R} u(t')\,\mathrm{d}t' \tag{2a}$$

If the laser spot is sufficiently large and has uniform pressure distribution, a one-dimensional impulse area density can be obtained

Table 1 Conditions of target

Material	Aluminum	POM
δ, μm	12–50	200–500
a_s, km/s	5.3	2.5
ρ, kg/m^3	$2.70 \cdot 10^3$	$1.41 \cdot 10^3$
τ_R, ns	4.5 ($\delta = 12$ μm)	160 ($\delta = 200$ μm)
τ_{1D}, μs	0.75 ($d = 8.0$ mm)	1.6 ($d = 8.0$ mm)
	0.26 ($d = 2.8$ mm)	——

Table 2 Conditions of laser

Laser	TEA CO_2	Nd:YAG
λ, μm	10.6	1.064
E, maximum value, J	10.3	0.90
τ_{FWHM}, ns	140	9
d, mm	8.0 (10.0 only in Figs. 13 and 14)	2.8

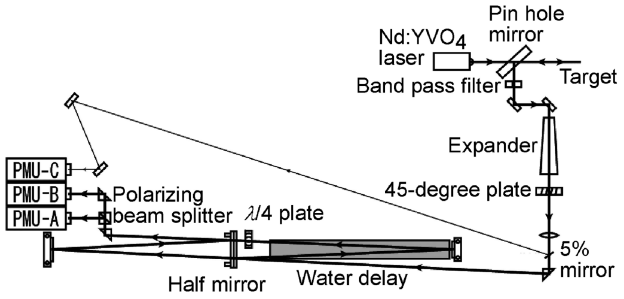

Fig. 2 Optical arrangement of VISAR.

from the rear surface velocity at the spot center. However, because the laser spot size is finite, even if the intensity is uniformly distributed, the one-dimensionality is violated when a wave released from the peripheral of the laser spot arrives at the center after a period of

$$\tau_{1D} = \frac{d}{2a_s} \tag{3}$$

In the following sections, the experimental data will be carefully analyzed by examining the applicability of Eq. (2).

III. Experimental Results

A. Effects of Target Thickness

In Figs. 3–5, the time variations of I_m for $P_0 = 100$ kPa obtained using Eq. (2) are plotted. In the case of the aluminum target, Figs. 3 and 4, ($\tau_R \cong \tau_V$) the reverberation motion is not resolved. The impulse area density can be obtained using Eq. (2) without averaging over each reverberation period. In Fig. 3, two repeat shots are plotted for each δ. In the case of $\delta = 25$ μm, the difference in the temporal value of I_m was less than 10% during the displayed period. However, for $\delta = 12$ μm, the reproducibility was not as good. In this study, shot-to-shot scatter to this extent could not be avoided. In Fig. 4, scatter in I_m were within 10%.

Only in the case of the TEA CO_2 laser pulse onto POM, Fig. 5a, the reverberation signals greatly superimpose on the impulse signals. However, when averaging over each reverberation period using Eq. (2a) (plotted as symbols in Fig. 5b), $\bar{I}_m$ is almost independent of δ; the scatter in its terminal value is less than 3%.

As will be seen later, I_m exhibited distinct sensitivity to the important control parameters, target material, type of laser, and ambient air pressure. Because most of the scatters in I_m were better than 10%, with a few up to 20%, detailed analyses of these parameters were possible with this level of reproducibility.

B. Dependence on Operation Conditions

Figures 6a–6c show the histories of I_m and corresponding momentum coupling coefficient C_m measured under various operation conditions. Here, C_m is defined by

$$C_m \equiv \frac{I_m}{\phi} \tag{4}$$

The variations with an aluminum target being irradiated with a TEA CO_2 laser pulse are shown in Fig. 6a. Unlike other cases (shown later), I_m gradually increased even during the laser power peak which is indicated with τ_{FWHM}. I_m and then C_m are increasing functions of the ambient pressure P_0. At $P_0 = 100$ kPa, C_m reached about 50 μN · s/J. For $P_0 < 1$ kPa, the velocity level was too low to be resolved with the present VISAR arrangement.

Figure 6b shows the variations with an aluminum target and an Nd:YAG laser pulse. Irrespective to the value of P_0, I_m sharply increased during the laser power peak. At high P_0, it continued to increase thereafter. I_m is also an increasing function of P_0. At $P_0 = 100$ kPa, the C_m level is about 30 μN · s/J, a little lower than that of Fig. 6a. What is different from Fig. 6a is that I_m did not vanish even at $P_0 = 10^{-2}$ Pa but increased in 50 ns.

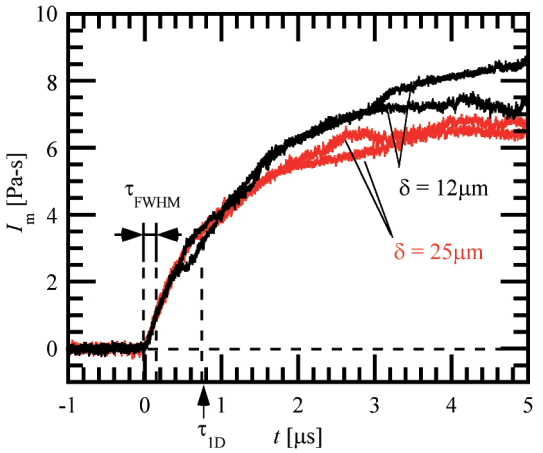

Fig. 3 Impulse histories measured at the spot center. TEA CO_2 laser irradiation on two different thickness Al targets: $E = 9.0$ J ($\phi = 17.9$ J/cm^2), $P_0 = 100$ kPa. Two repeat shots for the respective thickness targets are plotted.

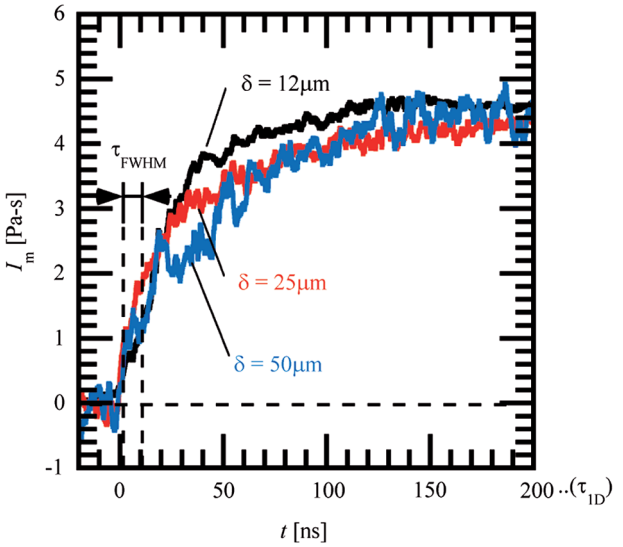

Fig. 4 Impulse histories measured at the spot center. Nd:YAG laser irradiation, $E = 890$ mJ ($\phi = 23.5$ J/cm^2) on three different thickness Al targets: $P_0 = 100$ kPa, $\tau_{1D} = 260$ ns is out of range.

Figure 6c shows the variations when a POM target is irradiated by a TEA CO_2 laser pulse. C_m exceeded 400 μN · s/J, which is of the same order as of [30], and one order of magnitude higher than that with the aluminum target (Fig. 6a). I_m most sharply increased during the primary power peak. Even thereafter it continued to increase. On one hand, at $P_0 = 100$ kPa, I_m saturated at about $t = 2$ μs. On the other hand, at $P_0 = 10^{-2}$ Pa, it continued to increase even $t > 4$ μs, attaining a higher value. Although this dependence on P_0 is opposite to the case of the aluminum target, it agrees with results of the free-flight experiments of Watanabe et al. [13]. Further discussions will be done in the next section.

IV. Discussions

A. Effective Period for Impulse Measurement

In this study, the rear surface velocity u was measured at the center of the laser irradiated spot. If the impulse generation is completed in $t < \tau_{1D}$, u is not affected by the boundary condition at the periphery of the laser spot and, using Eq. (2), this velocity can be readily related to the impulse area density at the laser spot center on the front surface I_m. In practice, the effective time period for the VISAR measurement is not necessarily equal to τ_{1D} for the following reasons: first, the laser intensity in the laser spot does not have a perfect flattop distribution

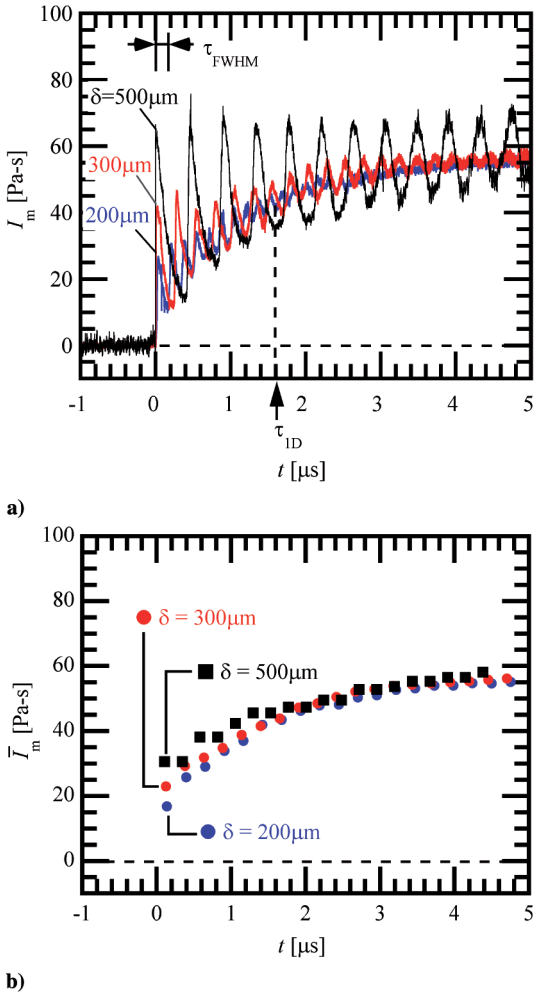

Fig. 5 Impulse histories measured at the spot center. TEA CO_2 laser irradiation, $E = 10.2$ J ($\phi = 13.0$ J/cm^2) on three different thickness POM targets: $P_0 = 100$ kPa, a) I_m, b) $\bar{I}_m$.

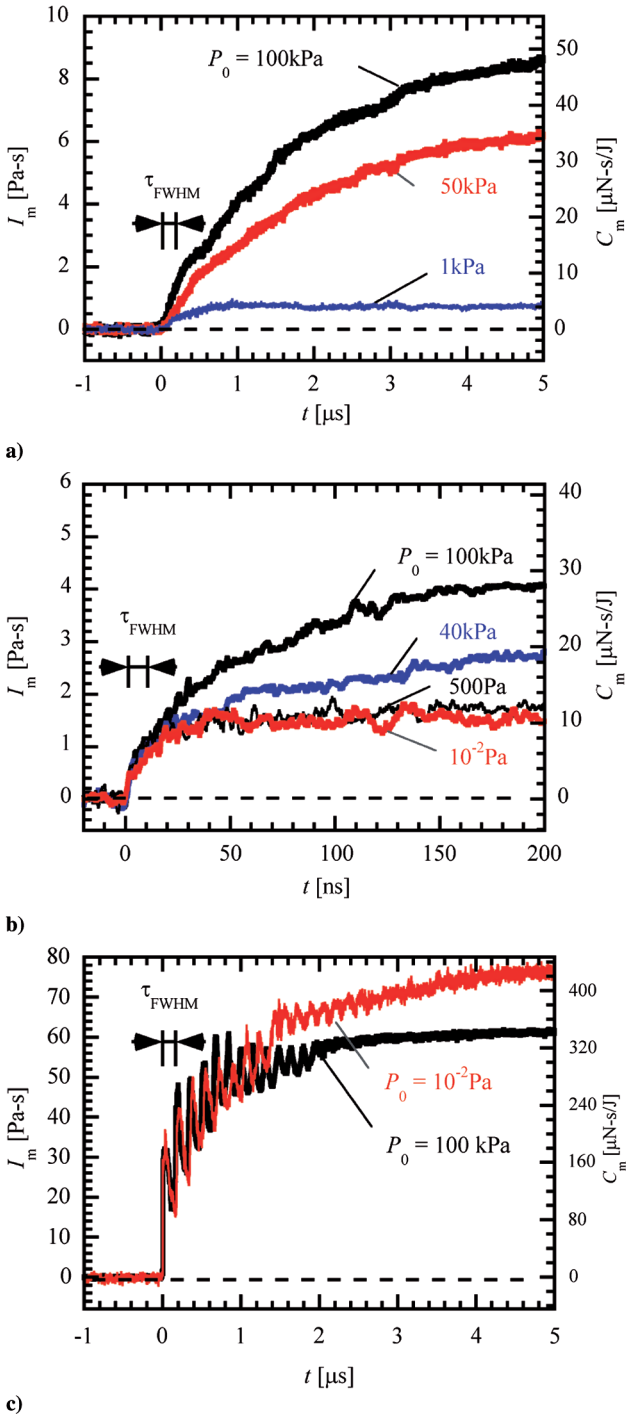

Fig. 6 Time variations of I_m and C_m: a) aluminum target ($\delta = 12$ μm) with TEA CO_2 laser ($E = 9.0$ J, $\phi = 17.9$ J/cm^2); b) aluminum target ($\delta = 12$ μm) with Nd:YAG laser ($E = 0.90$ J, $\phi = 14.5$ J/cm^2); c) POM target ($\delta = 200$ μm) with TEA CO_2 laser ($E = 9.0$ J, $\phi = 17.9$ J/cm^2).

over the laser spot; second, the pressure around the laser spot also increases so that the shear stress at the periphery is alleviated. Anyway, if the impulse continues to increase for a longer period of time, comparable to or greater than τ_{1D}, u is affected by the boundary conditions. In this situation, the correlation of u to I_m needs to be done carefully.

Because the penetration depth for the laser power into the target is smaller than the target thickness, in principle, the pressure on the front surface of the target is almost independent of the target thickness. However, after a long period of laser pulse irradiation, u is affected by the boundary conditions, and then by the target thickness δ. Therefore, the influence of δ is an appropriate criterion to validate the VISAR measurement. As seen in Figs. 3–5, the effective time period for Eq. (2) to have acceptable accuracy was experimentally examined through measurements of u for different thickness targets δ. In many cases, the laser-induced impulse is primarily generated during the power peak, which is characterized by its full width at half-maximum τ_{FWHM}. For all the conditions described in Figs. 3–5, $\tau_{\mathrm{FWHM}} \ll \tau_{1D}$. With the combination of the TEA CO_2 laser and the aluminum target (Fig. 3), the experimentally measured I_m for $t < 2\tau_{1D}$ is almost independent of δ. However, for $t \geq 1.5$ μs $= 2\tau_{1D}$, a later period in the same pulse, I_m of the thinner (12-μm-thick) target was larger than that of the thicker (25-μm-thick) one indicating that Eq. (2) was no longer completely valid. Because aluminum has a higher bulk sound speed than POM, see Table 1, and the laser pulse duration of the TEA CO_2 laser is more than one order in magnitude longer than the Nd:YAG laser pulse, see Table 2, the ratio $\tau_{1D}/\tau_{\mathrm{FWHM}}(=5.4)$ in Fig. 3 is the smallest among Figs. 3–5; the one-dimensionality is held shortest with respect to the peak power duration. In the case of Fig. 4 ($\tau_{1D}/\tau_{\mathrm{FWHM}} = 29$), I_m saturated in τ_{1D}; the scatter in the terminal value was within 10%. In the case of Fig. 5 ($\tau_{1D}/\tau_{\mathrm{FWHM}} = 11.4$), the scatter was 3%. Overall, the accuracy of Eq. (2) or (2a) is satisfactory to quantitatively discuss the effects of the important control parameters, except for such minor deviations as $t > 2\tau_{1D}$ in Fig. 3.

Because the ablation gas expands not only axially but also radially, high pressure is distributed outside of the laser spot on the front surface as well. This gaseous pressure field alleviates the tensile stress in the target around the laser spot periphery. Therefore, Eq. (2) or (2a) can remain accurate for an even longer period than τ_{1D}. If the impulse generation lasts much longer than τ_{1D}, special treatment is necessary to accurately measure the impulse area density. As will be

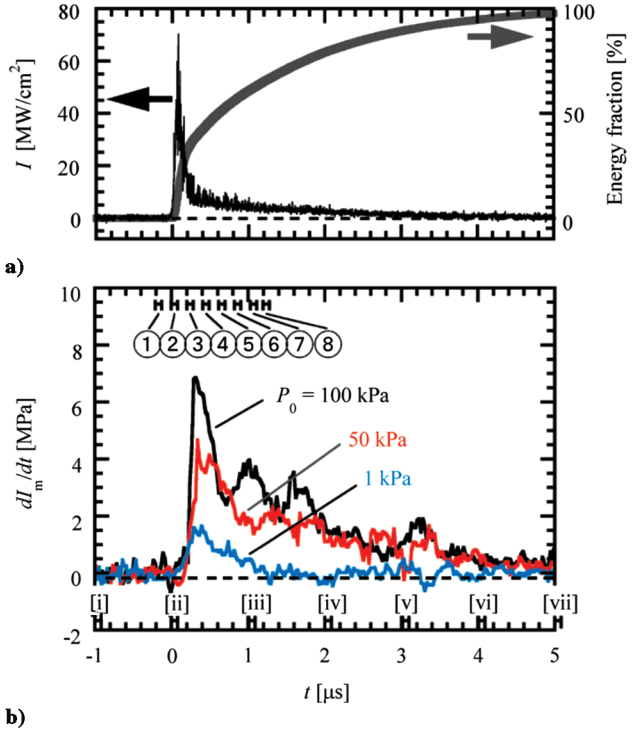

Fig. 7 Impulse generation processes on aluminum target with TEA CO_2 laser pulse, $E = 9.0$ J ($\phi = 17.9$ J/cm^2), $\delta = 12$ μm, same condition as in Fig. 6a: a) time variation of laser intensity I and integrated energy fraction, b) time variation of overpressure (time-derivative of I_m).

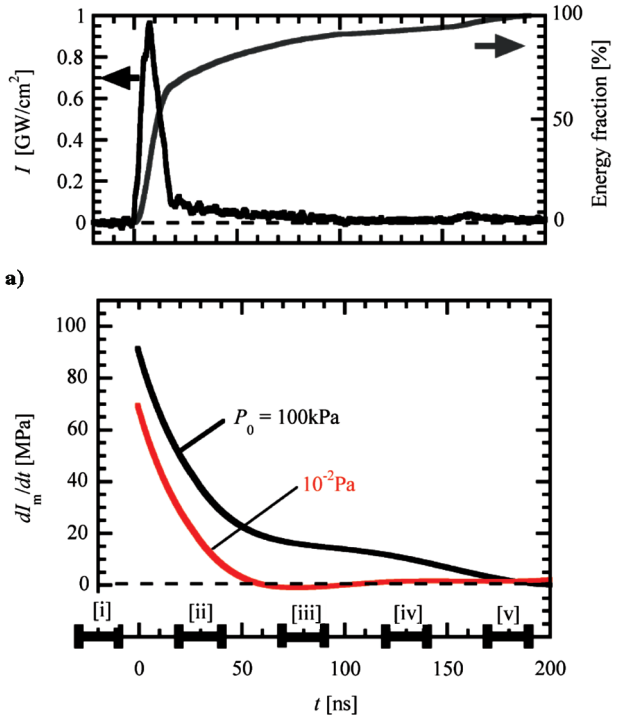

Fig. 9 Impulse generation processes on aluminum target with Nd:YAG laser, $E = 0.90$ J ($\phi = 14.5$ J/cm^2), $\delta = 12$ μm, same conditions as in Fig. 6b: a) time variation of I and integrated energy fraction, b) time variation of overpressure (smoothed).

shown later, such a situation occurred. The details will be presented in Sec. IV.D.

B. Impulse Generation Only Through Air Breakdown

Figures 7 and 8 show the detailed data of an aluminum target being irradiated with a TEA CO_2 laser pulse; the same condition as for Fig. 6a. As shown in Fig. 7a, the laser intensity I has a peak value I_{max} of 7×10^7 W/cm^2, with full width at half-maximum τ_{FWHM} of 140 ns. One-third of the total energy is delivered in 200 ns and 90% in 3.1 μm. The breakdown threshold for pure air in 10.6 μm light [33] is around 3×10^9 W/cm^2. In the present experiment, the peak value of the laser intensity is about two orders in magnitude lower than the nominal breakdown threshold. However, when the intensity is on the order of 10^7 W/cm^2 or higher, breakdown of the ambient air on the metal surface can occur [34,35]. This condition is satisfied here. The threshold intensity for ablation of aluminum in 10.6 μm light is on the order of 1×10^9 W/cm^2, which is more than one order of magnitude higher than I_{max} [36,37]. Ablation from the aluminum surface did not occur in this condition. The impulse was induced only by the breakdown of the ambient air near the target surface.

The preceding discussion is consistent with the results of the flow visualization shown in Fig. 8. In all cases, laser-induced air plasma is recognized as a radiating core. At $P_0 = 100$ and 50 kPa, a hemispherical shock wave is observed around the plasma. A high-pressure region is maintained behind the shock wave so that both the pressure and the duration time are increased. As a result, as seen in Fig. 7b, the overpressure level increased with increasing P_0. In other words, owing to the ambient air confinement, pressure was exerted on the target over an extended period from the laser pulse irradiation. At $P_0 = 1$ kPa, along the center axis above the target surface, the laser power absorption layer is coupled with a shock wave, which

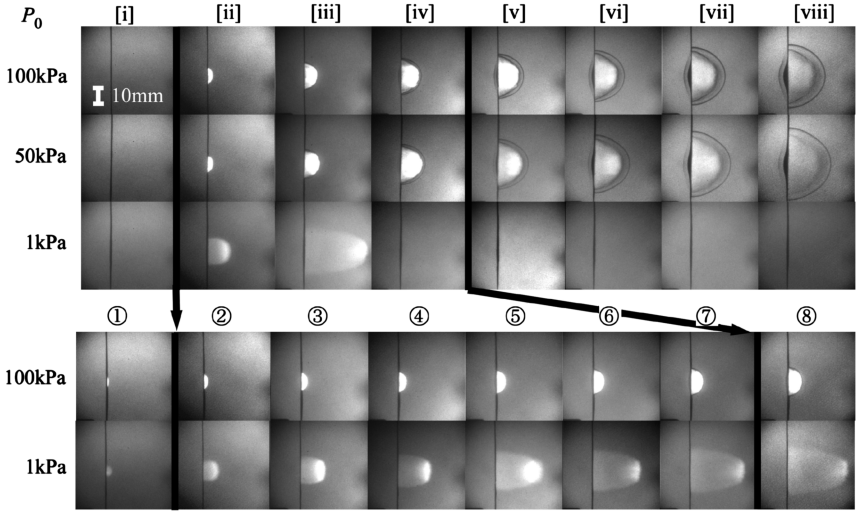

Fig. 8 Framing Schlieren images, same conditions as in Fig. 7, exposure 100 ns; frame timings are indicated in Fig. 7b.

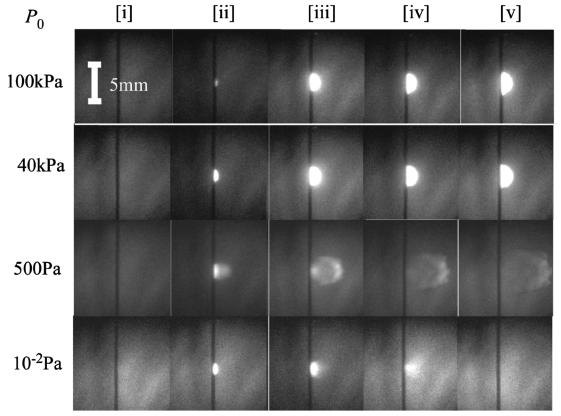

Fig. 10 Framing Schlieren images, same condition as in Fig. 9, exposure 20 ns; frame timings are indicated in Fig. 9b.

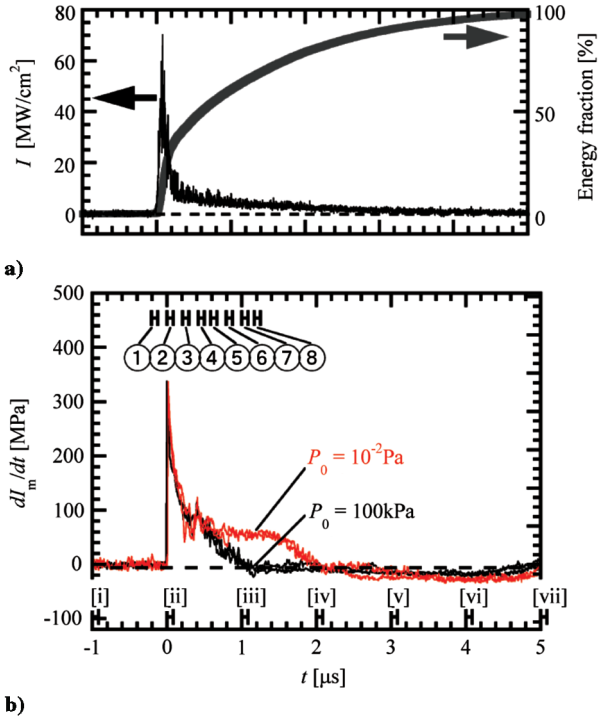

Fig. 11 Impulse generation processes on POM target with TEA CO_2 laser, $E = 9.0$ J ($\phi = 17.9$ J/cm^2), $\delta = 12$ μm, same conditions as in Fig. 6c: a) time variation of I and integrated energy fraction, b) time variation of overpressure which is measured with the target rear surface backed by the acrylic block.

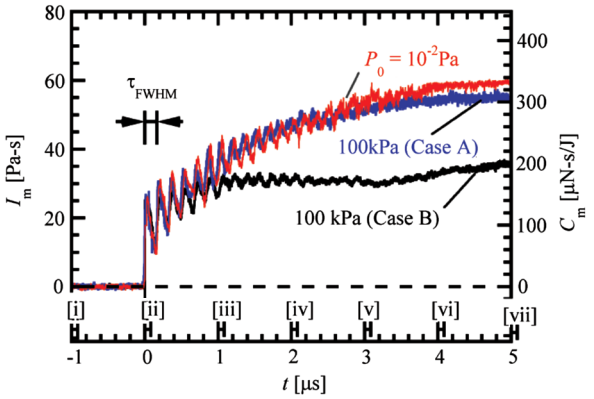

Fig. 13 Time variation of I_m, POM target with TEA CO_2 laser at $E = 10.3$ J ($d = 10$ mm, $\phi = 13.0$ J/cm^2), $\delta = 200$ μm, two modes (A: large impulse mode, B: small impulse mode) appeared, measured without acrylic block.

propagated forward at a speed of 20 km/s. However, this coupling and the overpressure terminated within 1 μs.

Dufresne et al. [29] reported that when an aluminum target was irradiated with a CO_2 laser pulse, the width of the pressure pulse decreased and the amplitude of the pressure peak increased with decreasing ambient air pressure. These reported tendencies contradict the present results. The peak intensity in this study was 7×10^7 W/cm^2, whereas, in their experiment, it was 1.5×10^8 W/cm^2. It does not seem reasonable to attribute these opposite pressure tendencies to this factor-of-two difference in laser intensity. Currently, this remains an open question, although the present experimental results do not seem questionable at all.

C. Impulse Generation Through Air Breakdown Assisted by Laser Ablation

Figures 9 and 10 show the detailed experimental data obtained using an Nd:YAG laser pulse, the same condition as for Fig. 6b. In this case, $I_{max} = 1.0 \times 10^9$ W/cm^2, exceeding by five times the ablation threshold of aluminum at the fundamental wavelength of the Nd:YAG laser, 1.064 μm. As is seen in Fig. 10, the ablation gas jet ejected from the target as a radiating flare, which contributed to the impulse generation even at the low P_0. Direct heating of the aluminum target causing the ablation jet occurred only during the primary laser intensity peak. The period of the interaction is relatively short, the order of $2\tau_{FWHM} \approx 20$ ns. The ambient air was not involved in the interaction during such a short period. The impulse was primarily generated due to the momentum of the ablation jet.

At atmospheric pressure, the high-pressure region driven by the ablated gas appeared and stayed for a much longer period than

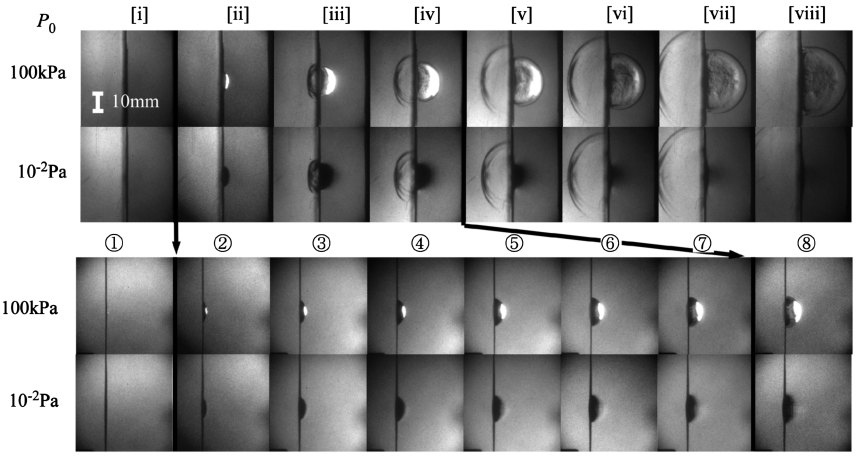

Fig. 12 Framing Schlieren images, same condition as in Fig. 11, exposure 100 ns; frame timings are indicated in Fig. 11b: upper: rear surface backed with acrylic block; lower: without acrylic block.

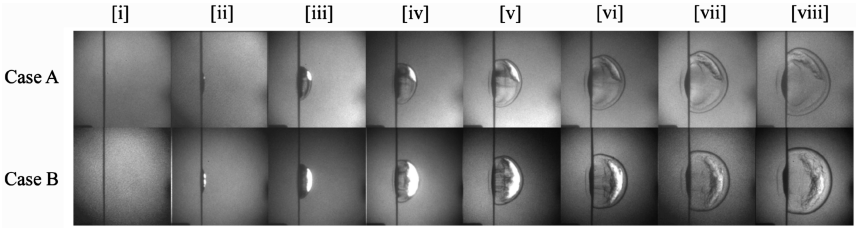

Fig. 14 Framing Schlieren images, same condition as in Fig. 13, exposure 100 ns; frame timings are indicated in Fig. 13.

τ_{FWHM}. The impulse was enhanced by this gas dynamic confinement. This ambient pressure dependence was similar to what was obtained in Sec. IV.B.

D. Ablation-Dominant Impulse Generation

Figures 11 and 12 show the detailed experimental data for TEA CO_2 laser pulse irradiation on a POM target, the same condition as for Fig. 6c. In this case, although $I_{\max} < 1.0 \times 10^8$ W/cm^2, an ablative jet was clearly observed as a dark plume in the Schlieren images of Fig. 12. Because the impulse continued to increase even when $t > \tau_{1D} = 1.6$ μs, the VISAR measurements were conducted with the POM target being backed by a 50-mm-thick acrylic block on its rear surface. The density, bulk sound speed, and acoustic impedance of POM are 1.41×10^3 kg/m^3, 2.5 km/s, and 3.53×10^6 kg m^{-2} s^{-1}, respectively; those of acrylic are 2.74×10^3 kg/m^3, 1.19 km/s, and 3.26×10^6 kg m^{-2} s^{-1}, respectively. Therefore, the acoustic impedances of these materials are matched within 8%. In this case, the experimentally measured u continues to correspond to the material velocity even after elastic waves transmit across the interface. In Fig. 11b, overpressure histories determined from u measured under the impedance matched condition are plotted. Two repeat shots are plotted for each P_0. At $P_0 = 100$ kPa, the overpressure monotonically decreased and vanished at $t = 1.3$ μs. However, at this instant, only 70% of the total laser energy was output. In the case of $P_0 = 10^{-2}$ Pa, the overpressure persisted longer: up to 2.1 μs.

In Fig. 12, a radiating layer is observed only at $P_0 = 100$ kPa. This layer presumably absorbed the proceeding laser power, shielding the target against direct energy transfer of the laser power. This phenomenon is commonly observed in other experiments, and is referred to as "plasma shielding." For $P_0 = 10^{-2}$ Pa, this residual portion of the laser energy is transferred onto the target surface more efficiently, thus the impulse continued to increase.

Figures 13 and 14 show the case of lower fluence. In this marginal condition, two modes appeared: one with strong plasma shielding, another with almost none. These events occurred sporadically. Without plasma shielding (case A), the radiated region was only partially observed. I_m continued to increase even for $t > 1$ μs, reaching a value of 55 Pa · s, close to that obtained at $P_0 = 10^{-2}$ Pa. However, with the strong plasma shielding (case B), the target was almost completely enveloped by the radiating layer. I_m saturated at $t = 1$ μs, reaching only 35 Pa · s. These results support the previously described interpretation of the effect of plasma shielding on the impulse generation.

Under the presented experimental conditions, the combinations of a POM target and a TEA CO_2 laser pulse yielded the highest momentum coupling coefficient. The impulse was generated primarily as the recoil of the ablation jet plume. Unlike the other cases, the ambient air had a negative impact due to plasma shielding.

V. Conclusions

In this study, the time variations of a propulsion impulse induced by a laser pulse on a target were measured using the VISAR with the time resolution of 4 ns. The fluence range was 13–24 J/cm^2. With the combination of aluminum target and TEA CO_2 laser, the laser intensity was lower than the ablation threshold. The target induced air breakdown near the surface. Without ablation, a relatively small impulse was obtained. With the combination of aluminum target and Nd:YAG laser, an ablation jet was ejected by the laser even at a low pressure, and an ablative impulse was obtained. In both cases, the impulse was an increasing function of P_0. The largest momentum coupling coefficient was obtained with the combination of POM target and TEA CO_2 laser. Only in this case, the impulse was larger at lower ambient pressure. At atmospheric pressure, the later portion of laser power was not efficiently transferred to the target surface because of plasma shielding. These results are consistent with the free-flight experiments of Watanabe et al. [13].

Acknowledgments

The authors cordially acknowledge valuable technical support from T. Ogawa, Technical Division, Institute of Fluid Science, Tohoku University and A. Saito, Technical Division, School of Engineering, Nagoya University. This research was supported by "Ground-Based Research Program for Space Utilization" promoted by Japan Space Forum, and by the Japan Society for Promotion of Science as KAKENHI (in Japanese), Grant-in-Aid for Scientific Research, No. 19206089.

References

[1] Kantrowitz, A., "Propulsion to Orbit by Ground-Based Lasers," *Astronautics and Aeronautics*, Vol. 10, No. 5, 1972, pp. 74–76.

[2] Pakhomov, A. V., and Gregory, D. A., "Ablative Laser Propulsion: An Old Concept Revisited," *AIAA Journal*, Vol. 38, No. 4, 2000, pp. 725–727.

[3] Phipps, C., "ORION, Challenges and Benefits," *Proceedings of High-Power Laser Ablation, The International Society for Optical Engineering*, Vol. 3343, International Society for Optical Engineering, Bellingham, WA, 1998, pp. 575–582.

[4] Phipps, C., Luke, J., Lippert, T., Hauer, M., and Wokaun, A., "Micropropulsion Using a Laser Ablation Jet," *Journal of Propulsion and Power*, Vol. 20, No. 6, 2004, pp. 1000–1011.

[5] Phipps, C., Turner, T. P., Harrison, R. F., York, G. W., Osborne, W. Z., Anderson, G. K., Colris, X. F., Haynes, L. C., Steele, H. S., Spicochi, K. C., and King, T. R., "Impulse Coupling to Targets in Vacuum by KrF, HF, and CO_2 Single-Pulse Lasers," *Journal of Applied Physics*, Vol. 64, No. 3, 1988, pp. 1083–1096. doi:10.1063/1.341867

[6] Phipps, C., Harrison, R. F., Shimada, T., York, G. W., Turner, T. P., Corlis, X. F., Steele, H. S., and Haynes, L. C., "Enhanced Vacuum Laser-Impulse Coupling by Volume Absorption at Infrared Wavelengths," *Laser and Particle Beams*, Vol. 8, Nos. 1–2, 1990, pp. 281–298.

[7] Pakhomov, A. V., Thompson, M. S., Swift, W., Jr., and Gregory, D. A., "Ablative Laser Propulsion: Specific Impulse and Thrust Derived from Force Measurements," *AIAA Journal*, Vol. 40, No. 11, 2002, pp. 2305–2311.

[8] Yabe, T., Phipps, C., Yamaguchi, M., Nakagawa, R., Aoki, K., Mine, H., Ogata, Y., Baasandash, C., Nakagawa, M., Fujiwara, E., Yoshida, K., Nishiguchi, A., and Kajiwara, I., "Microairplane Propelled by Laser Driven Exotic Target," *Applied Physics Letters*, Vol. 80, No. 23, 2002, pp. 4318–4320. doi:10.1063/1.1485313

[9] Yabe, T., Phipps, C., Aoki, K., Yamaguchi, M., Nakagawa, R., Baasandash, C., Ogata, Y., Shiho, M., Inoue, G., Onda, M., Horioka, K., Kajiwara, I., and Yoshida, K., "Laser-Driven Vehicles: From Inner-Space to Outer-Space," *Applied Physics A, Materials Science and Processing*, Vol. 77, No. 2, 2003, pp. 243–249.

[10] Knecht, S. D., Larson, C. W., and Mead, F. B., "Comparison of Ablation Performance in Laser Lightcraft and Standardized Mini-Thruster," *Proceedings of Fourth International Symposium on Beamed Energy Propulsion*, Vol. 830, American Inst. of Physics Melville, NY, 2006, pp. 615–627.

[11] Watanabe, K., and Sasoh, A., "Impulse Generation Using 300-J Class Laser with Confinement Geometries in Air," *Transactions of the Japan Society for Aeronautical and Space Sciences*, Vol. 48, No. 159, 2005, pp. 49–52. doi:10.2322/tjsass.48.49

[12] Phipps, C. R., and Michaelis, M. M., "LISP: Laser Impulse Space Propulsion," *Laser and Particle Beams*, Vol. 12, No. 1, 1994, pp. 23–54.

[13] Watanabe, K., Mori, K., and Sasoh, A., "Ambient Pressure Dependence of Laser-Induced Impulse of Polyacetal," *Journal of Propulsion and Power*, Vol. 22, No. 5, 2006, pp. 1150–1153. doi:10.2514/1.22750

[14] Tanaka, K. A., "Cryogenic Deutrrium Target Experiments with the GEKKO XII, Green Laser System," *Physics of Plasmas*, Vol. 2, No. 6, 1995, pp. 2495–2503. doi:10.1063/1.871211

[15] Koenig, M., Faral, B., Boudenne, J. M., Batani, D., Benuzzi, A., Bossi, S., Rémond, C., Perrine, J. P., Temporal, M., and Atzeni, S., "Relative Consistency of Equations of States by Laser Driven Shock Waves," *Physical Review Letters*, Vol. 74, No. 12, 1995, pp. 2260–2263. doi:10.1103/PhysRevLett.74.2260

[16] Da Silva, L. B., Celliers, P., Collins, G. W., Budil, K. S., Holmes, N. C., Barbee, T. W., Jr., Hammel, B. A., Kilkenny, J. D., Wallace, R. J., Ross, M., Cauble, R., Ng, A., and Chiu, G., "Absolute Equation of State Measurements on Shocked Liquid Deuterium up to 200 Gpa (2 Mbar)," *Physical Review Letters*, Vol. 78, No. 3, 1997, pp. 483–486. doi:10.1103/PhysRevLett.78.483

[17] Tanaka, K. A., Hara, M., Ozaki, N., Sasatani, Y., Anisimov, S. I., Kondo, K., Nakano, M., Nishihara, K., Takenaka, H., Yoshida, M., and Mima, K., "Multi-Layer Flyer Accelerated by Laser Induced Shock Waves," *Physics of Plasmas*, Vol. 7, No. 2, 2000, pp. 676–680. doi:10.1063/1.873851

[18] Berthe, L., Fabbro, R., Peyre, P., Tollier, L., and Bartnicki, E., "Shock Waves from a Water-Confined Laser-Generated Plasma," *Journal of Applied Physics*, Vol. 82, No. 6, 1997, pp. 2826–2832. doi:10.1063/1.366113

[19] Peyre, P., Berthe, L., Scherpereel, X., Fabbro, R., and Bartnicki, E., "Experimental Study of Laser-Driven Shock Waves in Stainless Steels," *Journal of Applied Physics*, Vol. 84, No. 11, 1998, pp. 5985–5992. doi:10.1063/1.368894

[20] Berthe, L., Fabbro, R., Peyre, P., and Bartnicki, E., "Wavelength Dependent of Laser Shock-Wave Generation in the Water-Confinement Regime," *Journal of Applied Physics*, Vol. 85, No. 11, 1999, pp. 7552–7555. doi:10.1063/1.370553

[21] Barker, L. M., and Hollenbach, R. E., "Laser Interferometer for Measuring High Velocities of Any Reflecting Surface," *Journal of Applied Physics*, Vol. 43, No. 11, 1972, pp. 4669–4675. doi:10.1063/1.1660986

[22] Remo, J. L., "High-Power-Pulsed 1054-nm Laser-Induced Shock Pressure and Momentum, and Energy Coupling to Iron-Nickel and Stony Meteorites," *Laser and Particle Beams*, Vol. 17, No. 1, 1999, pp. 25–44. doi:10.1017/S0263034699171039

[23] Pakhomov, A. V., Lin, J., and Tan, R., "Air Pressure Effect on Propulsion with Transversely Excited Atmospheric CO_2 Laser," *AIAA Journal*, Vol. 44, No. 1, 2006, pp. 136–141.

[24] D'Souza, B. C., and Ketsdever, A. D., "Investigation of Time-Dependent Forces on a Nano-Newton-Second Impulse Balance," *Review of Scientific Instruments*, Vol. 76, No. 015105, 2005.

[25] D'Souza, B. C., and Ketsdever, A. D., "Direct Impulse Measurement of Ablation Processes from Laser-Surface Interactions," AIAA Paper 2005-5172, June 2005.

[26] Schall, W. O., Eckel, H. A., Mayerhofer, W., Riede, W., and Zeyfang, "Comparative Lightcraft Impulse Measurement," *Proceedings of High-Power Laser Ablation 4*, Vol. 4760, International Society for Optical Engineering, Bellingham, WA, 2002, pp. 908–917.

[27] Gregg, D. W., and Thomas, S. J., "Momentum Transfer Produced by Focused Laser Giant Pulses," *Journal of Applied Physics*, Vol. 37, No. 7, 1966, pp. 2787–2789. doi:10.1063/1.1782123

[28] McMordie, J. A., and Roberts, P. D., "Interaction of Pulsed CO_2 Laser Radiation with Aluminium," *Journal of Physics D: Applied Physics*, Vol. 8, No. 7, 1975, pp. 768–781. doi:10.1088/0022-3727/8/7/009

[29] Dufresne, D., Bournot, Ph., Caressa, J. P., Bosca, G., and David, J., "Pressure and Impulse on an Aluminium Target from Pulsed Laser Irradiation at Reduced Ambient Pressure," *Applied Physics Letters*, Vol. 38, No. 4, 1981, pp. 234–236. doi:10.1063/1.92327

[30] Sterling, E., Lin, J., Sinko, J., Kodgis, L., Porter, S., Pakhomov, A. V., Larson, C. W., and Mead, F. B., Jr., "Laser-Driven Mini-Thrusters," *Proceedings of the 4th International Symposium on Beamed Energy Propulsion, AIP Conference Proceedings*, Vol. 830, American Inst. of Physics, Melville, NY, 2006, pp. 247–256.

[31] Mori, K., Anju, K., Sasoh, A., and Zaretsky, E., "Acceleration History in Laser-Ablative Impulse Measured Using Velocity Interferometer (VISAR)," *Proceedings of High-Power Laser Ablation 6*, Vol. 6261, International Society for Optical Engineering, Bellingham, WA, 2006, pp. 25-1–25-8.

[32] Barker, L. M., and Schuler, K. W., "Correction to the Velocity-Per-Fringe Relationship for the VISAR Interferometer," *Journal of Applied Physics*, Vol. 45, No. 8, 1974, pp. 3692–3693. doi:10.1063/1.1663841

[33] Morgan, C. G., "Laser-Induced Breakdown of Gases," *Reports on Progress in Physics*, Vol. 38, No. 5, 1975, pp. 621–665. doi:10.1088/0034-4885/38/5/002

[34] Pirri, A. N., Monsler, M. J., and Nebolsine, P. E., "Propulsion by Absorption of Laser Radiation," *AIAA Journal*, Vol. 12, No. 9, 1974, pp. 1254–1261.

[35] Ageev, V. P., Barchukov, A. I., Bunkin, F. V., Konov, V. I., Puzhaev, S. B., Silenok, A. S., and Chapliev, N. I., "Heating of Metals by CO_2 Laser Radiation Pulses," *Soviet Journal of Quantum Electronics*, Vol. 9, No. 1, 1979, pp. 43–47. doi:10.1070/QE1979v009n01ABEH008568

[36] Lin, J., Hughes, J., and Pakhomov, A. V., "Experimental Study of Coupling Coefficients for Propulsion on TEA CO_2 Laser," *Proceedings of Second International Symposium on Beamed Energy Propulsion*, Vol. 702, American Inst. of Physics, Melville, NY, 2004, pp. 122–128.

[37] Weyl, G. M., "Physics of Laser-Induced Breakdown: An Update," *Laser-Induced Plasmas and Applications*, edited by Radziemski, L. J., and Cremers, D. A., Marcel Dekker, New York, 1989, pp. 1–67.

G. Spanjers
Associate Editor